Anti-SIRPα antibody immunotherapy enhances neutrophil and macrophage antitumor activity

Nan Guo Ring[a,b,1], Dietmar Herndler-Brandstetter[b,1], Kipp Weiskopf[a,1], Liang Shan[b], Jens-Peter Volkmer[a], Benson M. George[a], Melanie Lietzenmayer[b], Kelly M. McKenna[a], Tejaswitha J. Naik[a], Aaron McCarty[a], Yunjiang Zheng[b], Aaron M. Ring[b,1], Richard A. Flavell[b,c,1,2], and Irving L. Weissman[a,1,2]

[a]Institute for Stem Cell Biology and Regenerative Medicine, and Ludwig Center for Cancer Stem Cell Research, Stanford University School of Medicine, Stanford, CA 94305; [b]Department of Immunobiology, Yale University School of Medicine, New Haven, CT 06520; and [c]Howard Hughes Medical Institute, New Haven, CT 06520

Contributed by Irving L. Weissman, October 13, 2017 (sent for review June 21, 2017; reviewed by Frederic Geissman and Hidde L. Ploegh)

Cancer immunotherapy has emerged as a promising therapeutic intervention. However, complete and durable responses are only seen in a fraction of patients who have cancer. A key factor that limits therapeutic success is the infiltration of tumors by cells of the myeloid lineage. The inhibitory receptor signal regulatory protein-α (SIRPα) is a myeloid-specific immune checkpoint that engages the "don't eat me" signal CD47 expressed on tumors and normal tissues. We therefore developed the monoclonal antibody KWAR23, which binds human SIRPα with high affinity and disrupts its binding to CD47. Administered by itself, KWAR23 is inert, but given in combination with tumor-opsonizing monoclonal antibodies, KWAR23 greatly augments myeloid cell-dependent killing of a collection of hematopoietic and nonhematopoietic human tumor-derived cell lines. Following KWAR23 antibody treatment in a human *SIRPA* knockin mouse model, both neutrophils and macrophages infiltrate a human Burkitt's lymphoma xenograft and inhibit tumor growth, generating complete responses in the majority of treated animals. We further demonstrate that a bispecific anti-CD70/SIRPα antibody outperforms individually delivered antibodies in specific types of cancers. These studies demonstrate that SIRPα blockade induces potent antitumor activity by targeting multiple myeloid cell subsets that frequently infiltrate tumors. Thus, KWAR23 represents a promising candidate for combination therapy.

cancer immunotherapy | SIRPA | myeloid cells | bispecific antibody | humanized mouse

Cancer immunotherapy utilizes the power and specificity of the host's immune system to eliminate malignant diseases and has become one of the most promising therapeutic interventions in the field (1–4). However, currently available immunotherapies face several obstacles that prevent complete and durable response rates in many patients who have cancer. For example, currently approved immunotherapies target only a fraction of tumor-infiltrating immune cells. Additive or synergistic treatment efficacy may therefore be achieved by targeting immune cells other than T and natural killer (NK) lymphocytes. In addition, tumor cells frequently develop resistance to chemotherapy and immunotherapy, which leads to incomplete tumor regression, dissemination, and metastasis of drug-resistant cancer cell clones (5, 6). In particular, cells of the myeloid lineage play a key role in limiting successful cancer therapy (7). Myeloid cells frequently infiltrate tumors, modulate tumor angiogenesis and inflammation, are associated with tumor resistance to chemotherapy and checkpoint blockade, and promote metastasis (8–13). One example of how tumor cells escape myeloid cell-dependent killing is to upregulate the antiphagocytic "don't eat me" signal CD47 (14). Whereas CD47 is expressed on tumors and normal tissues, its ligand, signal regulatory protein-α (SIRPα), has a limited expression pattern, with high levels of expression on macrophages, dendritic cells, neutrophils, and neurons (15, 16). SIRPα is a transmembrane protein with a cytoplasmic region containing immunoreceptor tyrosine-based inhibition motifs, which facilitate binding of the tyrosine phosphatases SHP-1 and SHP-2 (17). As such, SIRPα is a myeloid-specific immune checkpoint and represents a promising target for cancer immunotherapy. We therefore developed the anti-human SIRPα antibody KWAR23, analyzed its crystal structure and binding characteristics, and determined its therapeutic efficacy in eliminating tumor cells in vitro and in vivo. We further show that a bispecific anti-CD70/SIRPα antibody offers increased antitumor activity compared with individually administered antibodies in specific types of renal cancers. Together with antibodies that target tumor-infiltrating T and NK cell lineages, this anti-human SIRPα antibody may represent a promising candidate for combination therapies, which may achieve durable responses and may be more effective in treating metastatic cancers.

Results

Generation and Validation of Anti-Human SIRPα Antibody KWAR23. We obtained monoclonal antibodies against human SIRPα by immunizing mice and screening hybridomas for clones able to

Significance

Cancer immunotherapy is a promising therapeutic intervention. However, complete and durable responses are only seen in a fraction of patients who have cancer. Although cells of the myeloid lineage frequently infiltrate tumors and limit therapeutic success, currently approved immunotherapies primarily target tumor-infiltrating T and natural killer lymphocytes. The inhibitory receptor signal regulatory protein-α (SIRPα) represents a myeloid-specific immune checkpoint that engages the "don't eat me" signal CD47. Here, we developed an anti-human SIRPα antibody, KWAR23, which in combination with tumor-opsonizing antibodies, greatly augmented neutrophil and macrophage antitumor activity in vitro and in vivo. Thus, KWAR23 may represent a promising candidate for combination therapies and may achieve durable responses in a greater number of patients with cancer.

Author contributions: N.G.R., D.H.-B., K.W., L.S., J.-P.V., A.M.R., and R.A.F. designed research; N.G.R., D.H.-B., K.W., L.S., J.-P.V., B.M.G., M.L., K.M.M., T.J.N., A.M., Y.Z., and A.M.R. performed research; N.G.R., D.H.-B., K.W., L.S., J.-P.V., A.M.R., and I.L.W. analyzed data; and N.G.R., D.H.-B., K.W., A.M.R., R.A.F., and I.L.W. wrote the paper.

Reviewers: F.G., Memorial Sloan Kettering Cancer Center; and H.L.P., Boston Children's Hospital.

Conflict of interest statement: K.W., A.M.R., and I.L.W. are shareholders of Forty Seven, Inc., and have filed a patent application that describes the human anti-SIRPα antibody KWAR23. I.L.W. is co-inventor of the patent, and co-founder and director of the company that has licensed the antibody.

Data deposition: The atomic coordinates and structure factors of the KWAR23:SIRPα complex (PDB ID code 6BIT) have been deposited in the Protein Data Bank, www.wwpdb.org.

[1]N.G.R., D.H.-B., K.W., A.M.R., R.A.F., and I.L.W. contributed equally to this work.

[2]To whom correspondence may be addressed. Email: richard.flavell@yale.edu or irv@stanford.edu.

This article contains supporting information online at www.pnas.org/lookup/suppl/doi:10.1073/pnas.1710877114/-/DCSupplemental.

neutralize the interface between SIRPα and CD47 using a flow cytometric assay with yeast-displayed SIRPα and recombinant CD47. Clone KWAR23 showed strong expression and potent SIRPα antagonism, and was selected for further characterization. We determined the crystal structure of Fab fragments of KWAR23 bound to the IgV domain of human SIRPα (Fig. 1*A* and Table S1). Examination of the complex revealed that KWAR23 binds SIRPα at an epitope overlapping with the SIRPα/CD47 interface, indicating a basis for competitive antagonism of the SIRPα/CD47 interaction (Fig. 1*B*). A binding competition assay confirmed the specificity of the interaction between KWAR23 and SIRPα on the surface of THP-1 cells, a human acute monocytic leukemia cell line that expresses SIRPα (Fig. 1*C*). Surface plasmon resonance analysis of the binding kinetics of KWAR23 Fab fragments to the SIRPα IgV domain revealed high-affinity binding (K_d = 2.6–6.7 nM) to the two most prevalent alleles (Fig. 1 *D* and *E*). KWAR23 bound SIRPα expressed on human monocytes and neutrophils but minimally bound human B and T cells, which are known not to express SIRPα (Fig. 1*F*). The EC_{50} of KWAR23 binding to SIRPα on human $CD14^+$ monocytes was between 0.267 and 0.385 μg/mL (Fig. S1). In nonhuman primates, such as cynomolgus and rhesus macaques, KWAR23 bound SIRPα on $CD14^+$ monocytes with an EC_{50} of 0.338 and 0.4, respectively, which was comparable to the binding affinity in human donors.

KWAR23 Induces Human Macrophage-Dependent Phagocytosis in Human Tumor-Derived Cell Lines. We next evaluated the therapeutic activity of the anti-human SIRPα antibody KWAR23 alone or in combination with tumor-opsonizing antibodies, such as the anti-CD20 antibody rituximab (Fig. 2*A*). CD20-expressing Burkitt's lymphoma cells were incubated with human macrophages in vitro, and the phagocytosis index was measured after treatment with therapeutic antibodies. In combination with anti-CD20 antibodies (rituximab, obinutuzumab, or anti-CD20 antibodies of different Ig isotypes), KWAR23 significantly augmented phagocytosis of Burkitt's lymphoma cells (Fig. 2 *B*–*D*). Similarly, KWAR23 increased macrophage phagocytosis of DLD-1 colorectal adenocarcinoma cells opsonized by two different epidermal growth factor receptor (EGFR)-targeting antibodies, cetuximab and panitumumab, which differ in their heavy-chain isotypes (Fig. 2*E*). In combination with cetuximab, KWAR23 also increased phagocytosis of four different colon adenocarcinoma lines, regardless of downstream mutations in the EGFR signaling pathway (Fig. 2*F*). Notably, KWAR23 alone did not induce macrophage phagocytosis of nonopsonized tumor cells. These results indicate that the therapeutic activity of KWAR23 applies to hematopoietic and nonhematopoietic tumor cells, is driven by antibody-dependent cellular phagocytosis, and does not lead to generalized unspecific augmentation of phagocytosis.

KWAR23 Enhances Human Neutrophil and Macrophage Antitumor Activity in Vitro. Since both macrophages and neutrophils express SIRPα and are frequently found in tumors, they represent promising targets for anti-SIRPα antibody therapy. We therefore assessed the ability of human macrophages and neutrophils to kill opsonized tumor cells in vitro following treatment with KWAR23. Our antibody significantly augmented macrophage-mediated phagocytosis of carboxyfluorescein diacetate succinimidyl ester (CFSE)-labeled Burkitt's lymphoma cells, human epidermal growth factor receptor 2 (HER2)-expressing SK-BR-3 breast cancer cells, and DLD-1 colorectal adenocarcinoma cells following treatment with the anti-CD20 antibody rituximab, anti-HER2 antibody trastuzumab, or anti-EGFR antibody cetuximab (Fig. 3 *A*–*C*). Importantly, the effectiveness of KWAR23 to induce macrophage-mediated phagocytosis of tumor cells was dependent on an optimal concentration of tumor-opsonizing antibodies. Likewise, KWAR23 augmented neutrophil-mediated killing of CFSE-labeled

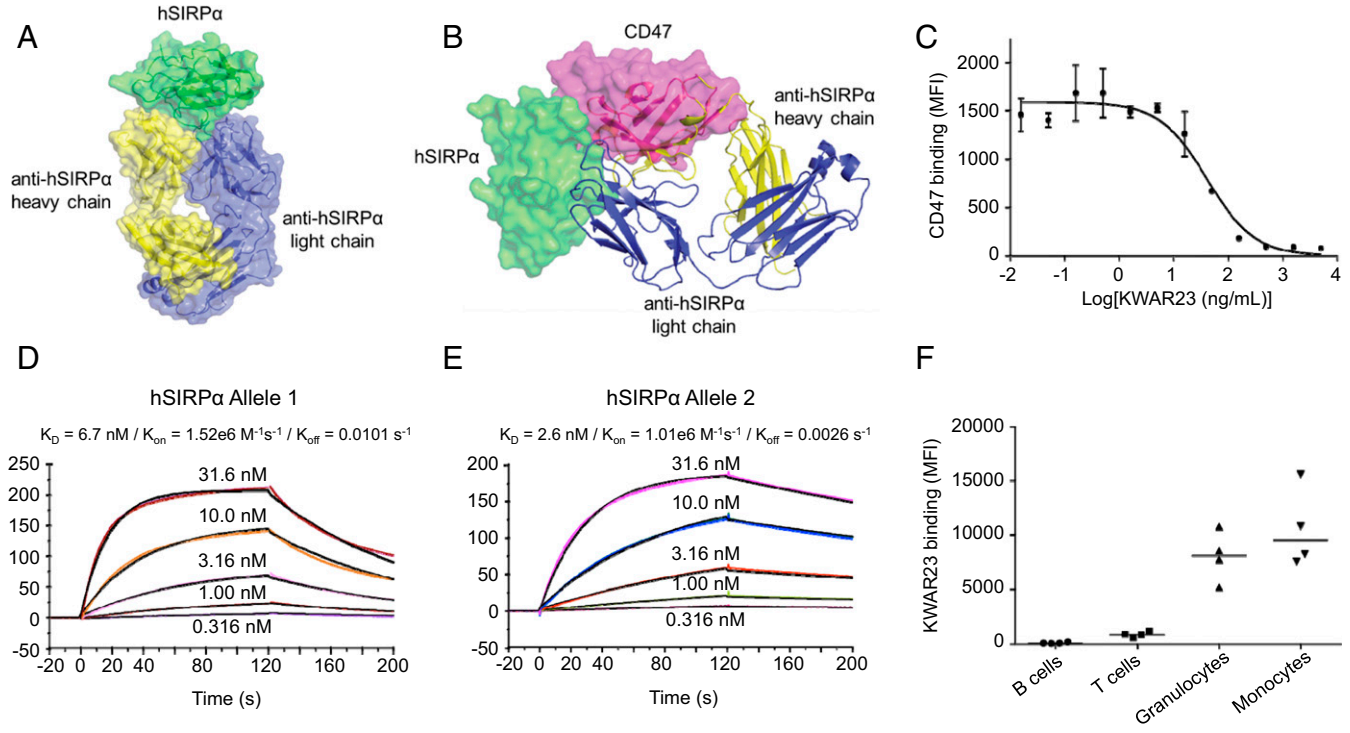

Fig. 1. Crystal structure and binding characteristics of the anti-human SIRPα antibody KWAR23. (*A*) Crystal structure of the KWAR23/SIRPα complex. (*B*) Overlay of the KWAR23/SIRPα and CD47/SIRPα complexes. KWAR23 Fab is depicted as ribbons, and the CD47/SIRPα complex is depicted as transparent surfaces. (*C*) Competition assay demonstrating KWAR23 blockade of CD47 binding to THP-1 cells. IC_{50} = 40.82 ng/mL. SD is shown. (*D* and *E*) Surface plasmon resonance analysis of the binding kinetics of KWAR23 Fab fragments to the two most prevalent alleles of the SIRPα IgV domain. (*F*) Binding of KWAR23 to human B cells, T cells, neutrophils, and monocytes. K_{off}, rate of dissociation; K_{on}, rate of association; MFI, mean fluorescence intensity.

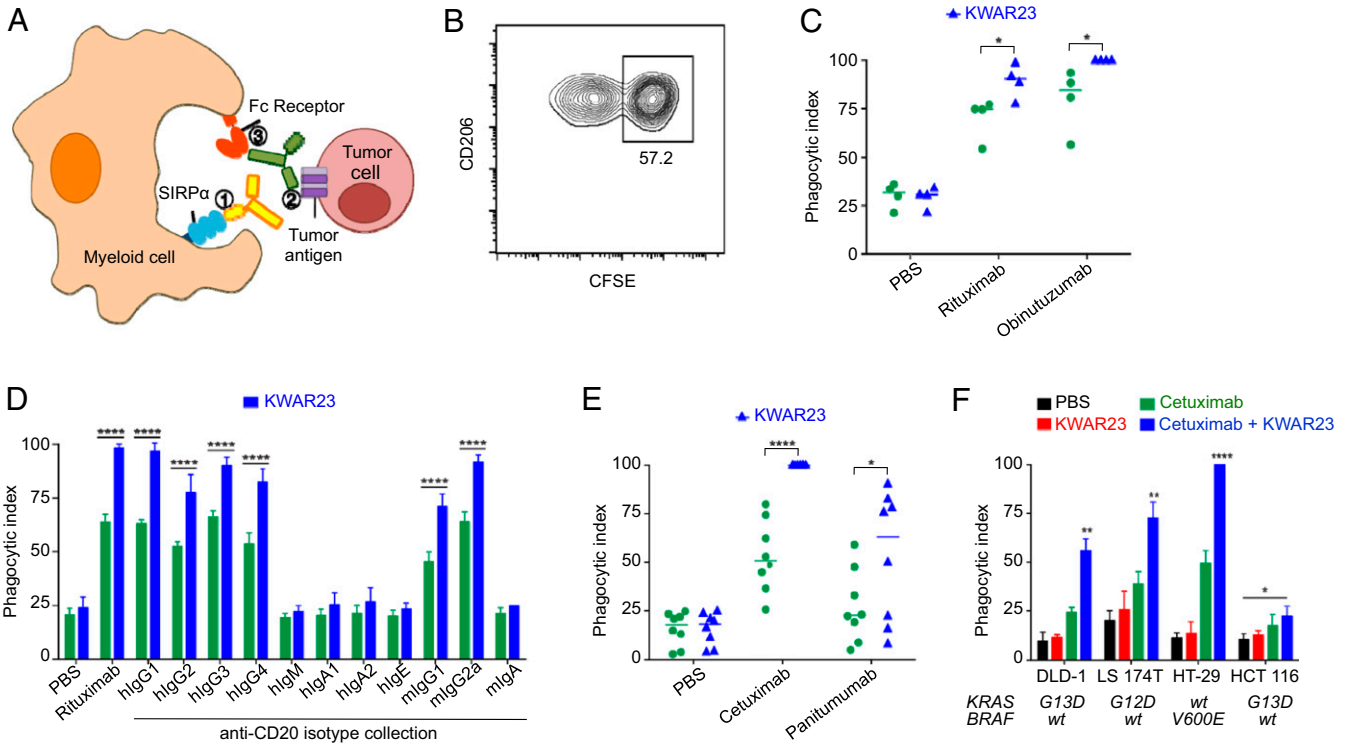

Fig. 2. Anti-human SIRPα antibody KWAR23 augments phagocytosis of tumor cells in vitro. (*A*) Schematic of myeloid cell-mediated phagocytosis of tumor cells by anti-SIRPα antibody and tumor-opsonizing antibodies (e.g., the anti-CD20 antibody rituximab). (*B*) Representative flow cytometry plot of a phagocytosis assay using human CD206$^+$ macrophages and CFSE-labeled tumor cells. (*C*) KWAR23 augments macrophage phagocytosis of Burkitt's lymphoma cells following treatment with two different CD20-targeting antibodies, rituximab and obinutuzumab. (*D*) KWAR23 increases monocyte phagocytosis of Burkitt's lymphoma cells opsonized by CD20-targeting antibodies across many Ig isotypes ($n = 4$). (*E*) KWAR23 enhances macrophage phagocytosis of DLD-1 colorectal adenocarcinoma cells opsonized by two different EGFR-targeting antibodies, cetuximab and panitumumab. (*F*) KWAR23 increases macrophage phagocytosis of four colon adenocarcinoma lines, regardless of *EGFR* pathway mutation status ($n = 4$). *wt*, wild type. Mean ± SEM is shown. *$P < 0.05$; **$P < 0.01$; ****$P < 0.0001$.

Burkitt's lymphoma cells and SK-BR-3 breast cancer cells following treatment with varying concentrations of rituximab or trastuzumab, respectively (Fig. 3 *D*–*F*). These results indicate that both human macrophages and neutrophils are capable of killing opsonized tumor cells following treatment with KWAR23. Furthermore, our data reveal the importance of optimizing concentrations of tumor-opsonizing antibodies to maximize the effectiveness of KWAR23-mediated tumor cell killing.

KWAR23 Exhibits Effective Antitumor Activity in a Human *SIRPA* Knockin Mouse Model. To evaluate the therapeutic activity of the anti-human SIRPα antibody KWAR23 in vivo, we employed a mouse model in which the extracellular domain of mouse *Sirpα* was replaced by human *Sirpα*, and we crossed this mouse to a *Rag2*$^{-/-}$ *Il2rg*$^{-/-}$ background (SRG mouse) (18). The homozygous knockin of human *Sirpα* corresponded to a knockout of mouse *Sirpα*. Flow cytometric analysis revealed high expression of human SIRPα on Ly6C^{hi} monocytes, Ly6G$^+$ neutrophils, F4/80$^+$ macrophages, and CD11c$^+$ dendritic cells, as well as high expression of human CD47 on Burkitt's lymphoma cells (Fig. S2).

We next performed s.c. engraftment of 5×10^6 Burkitt's lymphoma cells into the flank of SRG mice and initiated treatment with therapeutic antibodies upon visible formation of tumors (Fig. 4*A*). While treatment with rituximab or KWAR23 alone did not impact tumor growth, the combination of both antibodies led to strong inhibition of tumor growth in SRG mice (Fig. 4*B*). Long-term treatment (21 d) with rituximab and KWAR23 led to partial or complete remission in six of nine mice (Fig. 4*C*). The treatment of large tumors (170–300 mm^3) with rituximab and KWAR23 antibodies also led to significant reduction of tumor growth (Fig. 4*D*). Treatment with rituximab and KWAR23 did not affect the frequency of tumor-infiltrating cells (Fig. 4*E*). Of the CD45$^+$ tumor-infiltrating mouse cells, 25% were neutrophils and 40% were Ly6C^{hi} macrophages (Fig. 4 *F* and *G*). Antibody treatment did not affect the composition of tumor-infiltrating myeloid cell subsets. However, independent of treatment, we noticed a higher percentage of CD11c$^+$CD11b$^-$ dendritic cells and a slightly lower percentage of neutrophils in the tumor compared with peripheral blood (Fig. 4 *F* and *H*).

KWAR23 Enhances Neutrophil and Macrophage Antitumor Activity in SRG Mice. While macrophages have been shown to be successful targets for cancer immunotherapy, the role of neutrophils remains less characterized (19). To address the individual contributions of tumor-infiltrating macrophages and neutrophils to tumor growth inhibition by the KWAR23 antibody, we used clodronate to deplete phagocytic cells or an anti-Ly6G antibody to deplete neutrophils (Fig. 5*A*). Depletion of target populations in the blood before the start of the treatment was highly efficient (Fig. S3*A*), and the target populations were still absent in the blood and tumor at the end of the experiment (Fig. S3 *B* and *C*). Depletion of Ly6G$^+$ neutrophils in SRG mice treated with rituximab and KWAR23 led to increased tumor growth (Fig. 5*B*). Similarly, administration of clodronate, which removed CD11c$^+$CD11b$^+$ macrophages in the tumor (Fig. S3*C*), led to increased tumor growth (Fig. 5*B*). These results indicate that both macrophages and neutrophils frequently infiltrate tumors, are targets of anti-SIRPα antibody therapy, and are both capable of inhibiting tumor growth in vivo.

Therapeutic Activity of a Bispecific Anti-Human CD70/KWAR23 Antibody. We next determined whether KWAR23 could be combined with a tumor-opsonizing antibody other than rituximab, which would allow

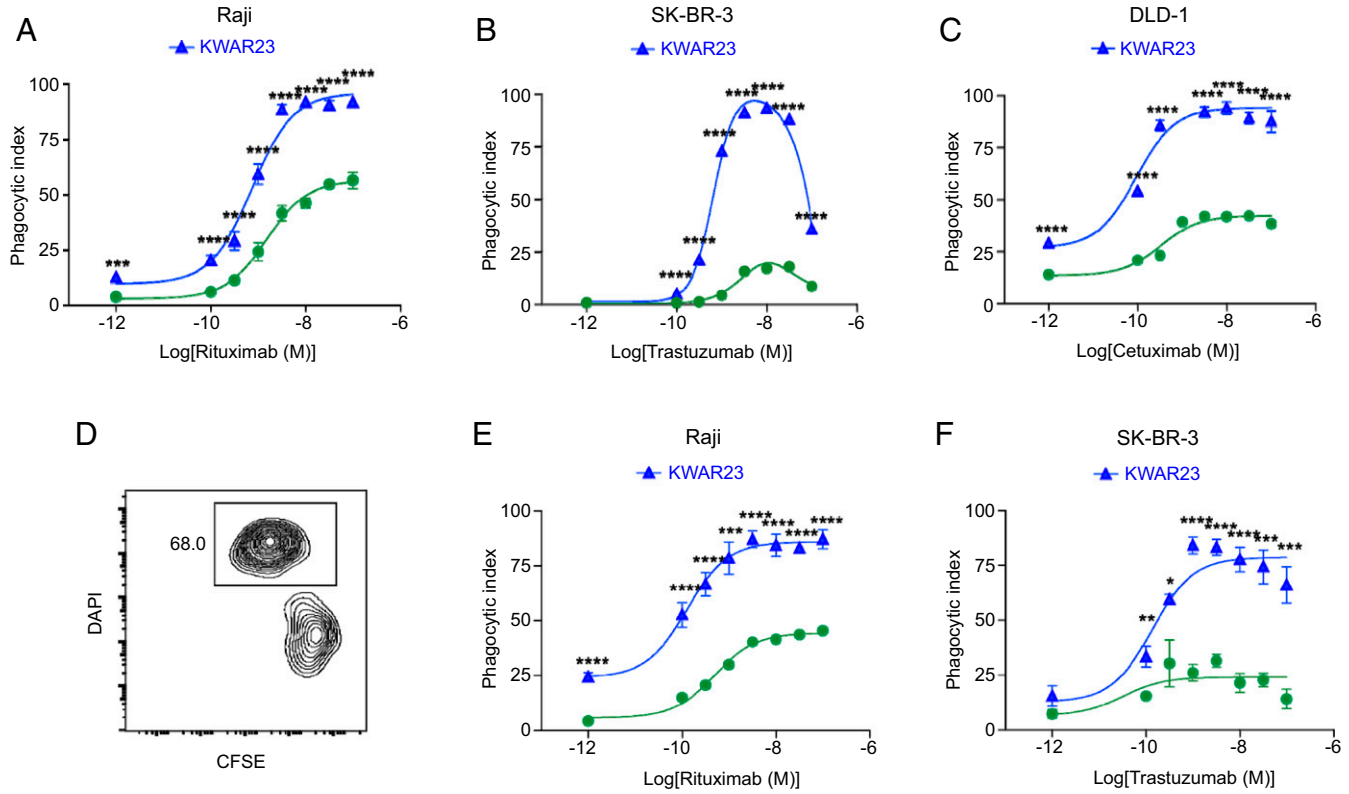

Fig. 3. KWAR23 augments macrophage- and neutrophil-mediated phagocytosis of tumor cells in vitro. (*A*) Phagocytosis of Burkitt's lymphoma cells by human macrophages following treatment with rituximab (green) or rituximab + KWAR23 (blue). Rituximab was provided at different concentrations as indicated on the abscissa ($n = 4$). (*B*) Phagocytosis of SK-BR-3 breast cancer cells by human macrophages following treatment with trastuzumab (green) or trastuzumab + KWAR23 (blue; $n = 4$). (*C*) Phagocytosis of colorectal adenocarcinoma (DLD-1) cells by human macrophages following treatment with cetuximab (green) or cetuximab + KWAR23 (blue; $n = 4$). (*D*) Representative flow cytometry plot of a cytotoxicity assay using human neutrophils and CFSE-labeled tumor cells. Dead cells were stained with DAPI. (*E*) Neutrophil-mediated killing of Burkitt's lymphoma cells following treatment with rituximab (green) or rituximab + KWAR23 (blue; $n = 4$). (*F*) Neutrophil-mediated killing of SK-BR-3 breast cancer cells following treatment with trastuzumab (green) or trastuzumab + KWAR23 (blue; $n = 4$). Mean ± SEM is shown. $*P < 0.05$; $**P < 0.01$; $***P < 0.001$; $****P < 0.0001$.

treatment of tumors that do not express CD20. Human CD70 is an antigen with limited expression in normal cells but high expression in malignancies, such as non-Hodgkin lymphoma, multiple myeloma, renal cell carcinoma, and glioblastoma (20, 21). Thus, anti-CD70 antibodies are being pursued as a therapeutic target for cancer immunotherapy (22, 23). Since CD70 is expressed on most B cell malignancies, including Burkitt's lymphoma cells (Fig. S2*B*), we injected Burkitt's lymphoma cells into SRG mice and treated them with the anti-CD70 antibody vorsetuzumab and KWAR23. Similar to our results with rituximab, treatment with vorsetuzumab and KWAR23 led to strong inhibition of tumor growth in SRG mice (Fig. 5*C*). These results demonstrate that KWAR23 can be combined with antibodies that target different tumor antigens, thereby broadening the application of anti-SIRPα cancer immunotherapy.

Bispecific monoclonal antibodies, which are fusion proteins that bind two different antigens, have been developed to facilitate engagement of the immune system (24). By binding multiple antigens simultaneously, they can increase avidity, enhance Fc-receptor engagement, and further bridge effector and target cells. We therefore developed a bispecific anti-human CD70/KWAR23 antibody (Table S2) and compared its therapeutic efficacy with that of the individually administered monoclonal antibodies. In vitro experiments show that KWAR23 only moderately induced macrophage phagocytosis of four different renal carcinoma cell lines (RCC4, RCC10, TK10, and Caki-1) following incubation with the anti-human CD70 antibody vorsetuzumab (Fig. 5*D*). However, the bispecific anti-human CD70/KWAR23 antibody significantly enhanced phagocytosis of RCC10 and TK10 renal carcinoma cells, compared with treatment with vorsetuzumab or the combination of vorsetuzumab and KWAR23. KWAR23 or anti-CD47 alone did not induce macrophage phagocytosis of nonopsonized tumor cells compared with PBS treatment. In vivo, the bispecific antibody effectively inhibited Burkitt's lymphoma cell growth in SRG mice, but did not outperform the combination of the two individual therapeutic antibodies (Fig. 5*C*). These results indicate that a bispecific anti-human CD70/KWAR23 antibody enhances tumor cell killing of certain cancers, and may outperform individually administered antibodies in these cases.

Discussion

With numerous tumor-opsonizing antibodies and checkpoint inhibitors approved and even more agents under evaluation for clinical use, antibody-based therapy for cancer has become one of the most successful and important strategies for treating patients with malignancies (25). However, a major challenge in the field of cancer immunotherapy is that complete and durable responses are only achieved in a fraction of patients with cancer. Combination immunotherapy, which targets not only different regulatory pathways in immune and cancer cells but also different types of tumor-infiltrating immune cells, may represent a promising approach to induce a rapid and durable antitumor response and prevent therapy-induced resistance, dissemination, and metastasis of cancer cells (26). Although myeloid cells frequently infiltrate tumors, modulate tumor angiogenesis, are associated with tumor resistance to chemotherapy and immune

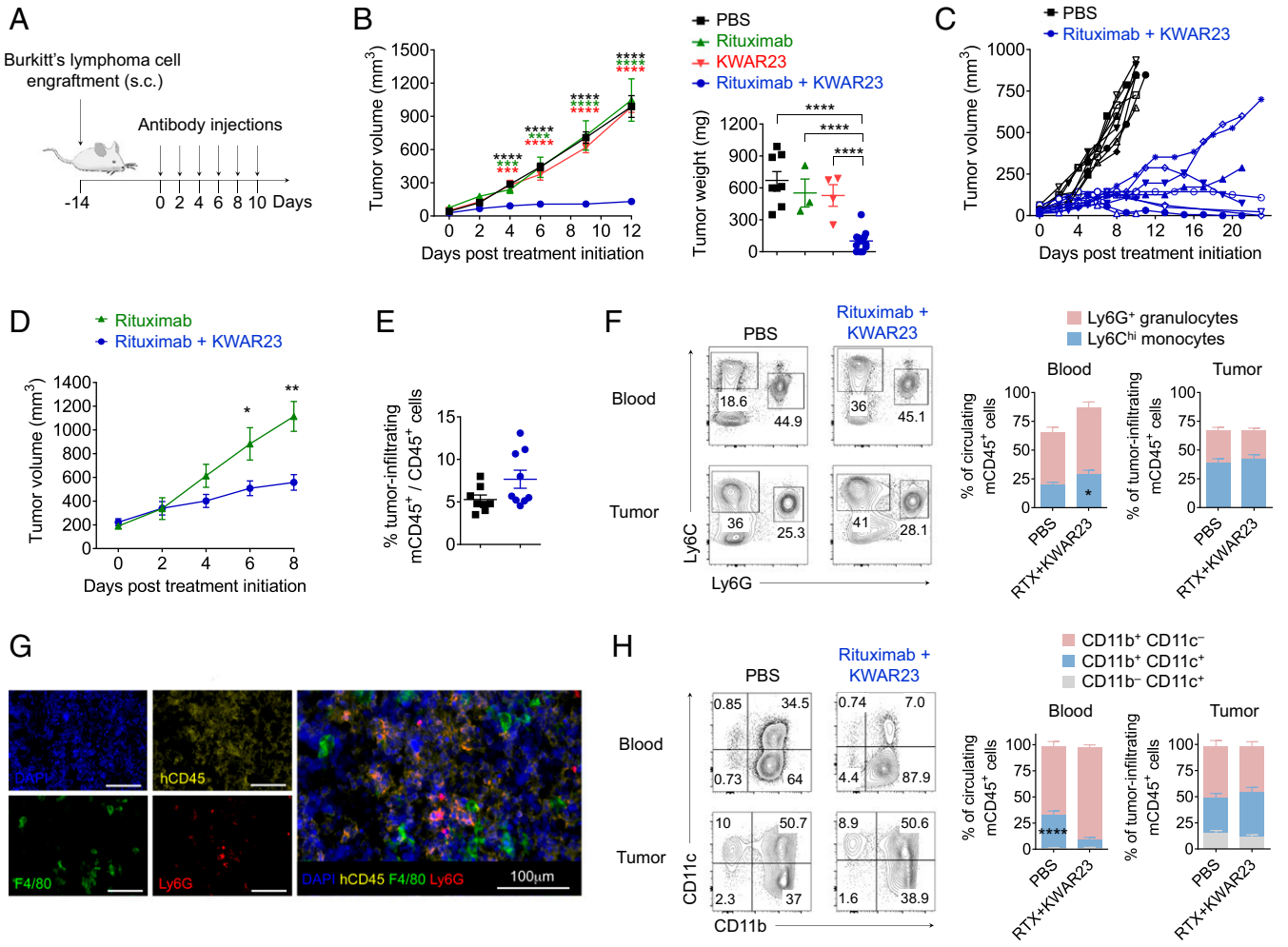

Fig. 4. Therapeutic activity of KWAR23 in SRG mice. (*A*) Schematic of the tumor engraftment and immunotherapy in SRG mice. (*B*) Tumor volume and weight in SRG mice treated with PBS ($n = 8$), rituximab ($n = 3$), KWAR23 ($n = 4$), or rituximab + KWAR23 ($n = 14$). The color of the stars indicates comparison of the corresponding group with the rituximab + KWAR23 group. (*C*) Individual tumor growth curves in SRG mice treated with PBS ($n = 9$) or rituximab + KWAR23 ($n = 12$). (*D*) SRG mice that established large tumors (170–300 mm^3) were treated for 8 d with rituximab ($n = 4$) or rituximab + KWAR23 ($n = 4$). (*E*) Frequency of tumor-infiltrating mouse $CD45^+$ cells in SRG mice treated with PBS ($n = 9$) or rituximab + KWAR23 ($n = 8$). (*F*) Frequency of $Ly6C^{hi}$ $Ly6G^-$ macrophages and $Ly6G^+$ $Ly6C^{dim}$ neutrophils in the blood and tumor of SRG mice treated with PBS ($n = 8$) or rituximab + KWAR23 ($n = 9$). (*G*) Immunofluorescence images showing the infiltration of human Burkitt's lymphoma xenografts (human $CD45^+$) in rituximab + KWAR23-treated SRG mice by $F4/80^+$ macrophages and $Ly6G^+$ neutrophils. (*H*) Frequency of dendritic and myeloid cells in the blood and tumor of SRG mice treated with PBS ($n = 8$) or rituximab + KWAR23 ($n = 9$). Mean ± SEM is shown. $*P < 0.05$; $**P < 0.01$; $****P < 0.0001$ (unpaired two-tailed Student's *t* test).

checkpoint blockade, and promote metastasis (8, 10), an immunotherapeutic approach that specifically targets myeloid cell subsets has not been clinically approved.

The CD47/SIRPα axis is emerging as one of the most promising new immunotherapeutic targets, and a number of clinical trials are now underway to evaluate CD47/SIRPα blocking therapies (27). All agents currently under clinical investigation target CD47 directly. Since CD47 is ubiquitously expressed on normal cells throughout the body, this raises the potential for on-target toxicity to healthy cells and a large "antigen sink." Given its more restricted tissue expression, direct targeting of SIRPα provides a potential strategy to overcome these obstacles.

We therefore developed the monoclonal antibody KWAR23, which binds human SIRPα with high affinity and disrupts its binding to CD47. Administered by itself, KWAR23 was inert, but given in combination with the tumor-opsonizing antibody rituximab, KWAR23 greatly enhanced antibody-dependent killing of a human tumor xenograft in SRG mice. The finding that KWAR23 alone did not enhance myeloid cell-mediated killing of tumor cells may be indicative of a favorable side-effect profile. Mice treated with KWAR23 did not show any immune cell infiltrates in the brain and did not exhibit any apparent neurological abnormalities. This is in accordance with studies of SIRPα knockout mice, which did not manifest any embryonic or postnatal developmental deficiencies (28). Treatment with vorsetuzumab and KWAR23 augmented macrophage-dependent phagocytosis of renal carcinoma cells in vitro and outperformed treatment with an anti-human CD47 antibody (Fig. 5*D*). These results indicate that although targeting CD47 may offer additional SIRPα-independent effects, KWAR23 represents a highly effective myeloid-specific checkpoint inhibitor. In vitro experiments also showed that targeting CD47/SIRPα interactions in human neutrophils potentiated trastuzumab-mediated antibody-dependent cellular cytotoxicity (ADCC) against breast cancer cells (29). By using syngeneic mouse models, another study showed that an anti-mouse SIRPα antibody attenuated the growth of SIRPα-expressing renal cell carcinoma and melanoma cells (30). Whereas these studies indicate that SIRPα is a promising new immunotherapeutic target, our study demonstrates the in vivo antitumor activity of neutrophils and macrophages in a human *SIRPA* knockin mouse model following treatment with an

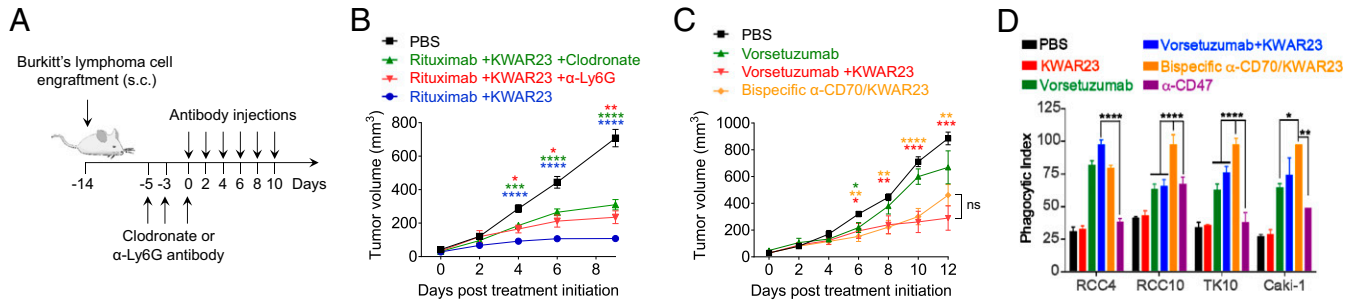

Fig. 5. KWAR23 augments macrophage- and neutrophil-mediated destruction of human tumor xenografts in SRG mice. (*A*) Schematic of the tumor engraftment, depletion of myeloid cell subsets, and immunotherapy in SRG mice. (*B*) Impact of the depletion of myeloid cell subsets on tumor growth in SRG mice treated with PBS ($n = 8$), rituximab + KWAR23 + clodronate ($n = 12$), rituximab + KWAR23 + anti-Ly6G ($n = 8$), and rituximab + KWAR23 ($n = 9$). The color of the stars indicates comparison of the PBS group with the corresponding treatment group. (*C*) Tumor growth in SRG mice treated with PBS ($n = 7$), vorsetuzumab ($n = 3$), vorsetuzumab + KWAR23 ($n = 5$), or bispecific anti-CD70/KWAR23 ($n = 6$). The color of the stars indicates comparison of the PBS group with the corresponding treatment group. ns, not significant. (*D*) Phagocytosis of four different renal carcinoma cells by human macrophages following treatment with vorsetuzumab, vorsetuzumab + KWAR23, bispecific anti-human CD70/KWAR23, and anti-human CD47 antibody ($n = 4$). Mean ± SEM is shown. $*P < 0.05$; $**P < 0.01$; $***P < 0.001$; $****P < 0.0001$ (unpaired two-tailed Student's *t* test).

anti-human SIRPα antibody. In addition, we demonstrate that a bispecific anti-human CD70/SIRPα antibody outperforms individually administered antibodies in certain types of cancers.

Remarkably, the potent antitumor activity of KWAR23 in SRG mice was achieved in the absence of T, B, and NK cells. Tumor-opsonizing antibodies, such as rituximab, have been shown to induce killing of cancer cells via antibody-dependent cellular cytotoxicity by NK cells (31). CD47 blockade has also been reported to trigger T cell-mediated destruction of immunogenic tumors, for example, by enhancing cytosolic sensing of tumor cell-derived DNA in a stimulator of interferon genes (STING)-dependent manner (32, 33). These studies suggest that the efficacy of treatment with rituximab and KWAR23 observed in our SRG mouse model is likely to be even higher in the presence of NK and T cells. A recent study showed that macrophages were more efficient at phagocytosis of hematopoietic than nonhematopoietic tumor cells, in response to SIRPα-CD47 blockade, which depended on the ability of SLAMF7 to interact with the integrin Mac-1 (34). However, our results indicate that combination treatment of KWAR23 with a tumor-opsonizing antibody was highly efficient in killing both hematopoietic (Raji) and nonhematopoietic (colorectal adenocarcinoma, mammary gland carcinoma, and renal carcinoma) human tumor-derived cell lines. Importantly, the therapeutic success of KWAR23 treatment was independent of the EGFR pathway mutation status in four different colon adenocarcinoma lines, highlighting the potential of KWAR23 as a universal candidate for combination therapy in patients with tumor-infiltrating myeloid cells.

Several studies have shown that the depletion of specific myeloid cell subsets, such as neutrophils, macrophages, and myeloid-derived suppressor cells, inhibits tumor growth and improves the efficacy of checkpoint blockade (7, 35–38). However, myeloid cells themselves are able to kill tumor cells, and leukemia cells, for example, up-regulate CD47 to avoid macrophage-mediated phagocytosis (14). In addition, macrophages and dendritic cells play a key role in presenting tumor cell-derived antigens to $CD8^+$ and $CD4^+$ T cells, thereby supporting T cell-mediated destruction of tumor cells (39–41). Instead of depleting antigen-presenting phagocytic cells, which may also eliminate potential beneficial effects, we utilized the large number of myeloid cells in the tumor environment to specifically enhance their antitumor activity by using KWAR23. Interestingly, our results suggest that treatment with rituximab and KWAR23 in SRG mice was more effective in inhibiting tumor growth than the depletion of neutrophils or phagocytic cells. This does not even take into account any additive or synergistic effects that may be conveyed by T, B, or NK cells.

In summary, we show that KWAR23 binds with high affinity to SIRPα expressed on human myeloid cell subsets, thereby blocking SIRPα-mediated inhibitory signaling and augmenting killing of antibody-opsonized tumor cells. Our results further demonstrate that KWAR23 targets neutrophils and macrophages, and that both of these cell subsets contribute to tumor growth inhibition in vitro and in vivo. SIRPα blockade thus represents a promising approach in cancer immunotherapy as it targets multiple myeloid cell populations, which frequently infiltrate tumors, promote tumor metastasis, and mediate resistance to chemotherapy and checkpoint blockade (11, 35, 42, 43). Together with therapeutic antibodies that target other tumor-infiltrating immune cells, our KWAR23 antibody represents a promising candidate for combination therapies that may facilitate rapid and complete elimination of tumors. Since neutrophils and macrophages are critically important for the dissemination and metastatic colonization of circulating tumor cells (44), the KWAR23 antibody may also be more effective in treating locally invasive and metastatic cancers.

Materials and Methods

Generation of Anti-Human SIRPα Antibody KWAR23. Mice were immunized with the recombinant IgV domain of human SIRPα (allele 1) by AbPro, Inc., with a proprietary adjuvant formulation and immunization schedule. Hybridoma supernatants were screened for SIRPα binding and CD47 blockade by application to yeast displaying human SIRPα and secondary staining with anti-mouse IgG and the biotinylated Ig domain of CD47. Clone KWAR23 exhibited high expression yield and potent SIRPα blockade and was selected for further characterization. The KWAR23 heavy- and light-chain V-region sequences were obtained by 5′-RACE PCR of hybridoma cDNA by Genscript. The amino acid sequences of the KWAR23 V-regions are shown in Table S2.

Protein Expression and Purification. KWAR23 antibody was purified by protein A chromatography (Thermo Fisher Scientific) from hybridoma supernatants grown in CELLine CL1000 bioreactors (Sigma). The IgV domain of human SIRPα and Ig domain of CD47 were prepared from *Escherichia coli* and *Trichoplusia ni* (*T. ni*) insect cells as previously described (45). Biotinylated SIRPα and CD47 were prepared by in vitro biotinylation of C-terminally avi-tagged (GLNDIFEAQKIEWHE) material using BirA ligase as previously described (45). Bispecific antibodies were prepared by transient transfection of HEK293F cells using 293Fectin (Thermo Fisher Scientific) according to the manufacturer's instructions and purification by protein A chromatography. KWAR23 Fab fragments were prepared by digestion with immobilized ficin (Pierce) according to the manufacturer's instructions. Undigested antibody and Fc fragments were removed by protein A chromatography, and Fab fragments were further purified by size-exclusion chromatography over a 10/300 S200 column (GE Healthcare). All proteins for in vivo or cellular studies were

buffer-exchanged into sterile PBS using PD-10 columns (GE Healthcare). KWAR23 Fab/SIRPα IgV complexes for crystallization were prepared by addition of equimolar 8× histidine-tagged SIRPα IgV to ficin-digested KWAR23 Fabs. Complexes were purified by nickel-nitrilotriacetic acid chromatography, digested with Carboxypeptidases A and B (Sigma), and polished by size-exclusion chromatography with a 10/300 S200 column into HBS [10 mM Hepes (pH 7.4), 150 mM NaCl].

Surface Plasmon Resonance. Experiments were conducted with a Biacore T100 system at 25 °C. Protein concentrations were quantified by 280-nm absorbance with a Nanodrop2000 spectrometer (Thermo Fisher Scientific). A Biacore SA sensor chip (GE Healthcare) was used to capture biotinylated SIRPα IgV, allele 1 or 2 [maximal resonance units $R_{max} \sim 200$ resonance units (RU)]. An unrelated biotinylated protein was immobilized with an RU value matching that of the reference surface to control for nonspecific binding. Measurements were made with serial dilutions of the KWAR23 Fab in HBS-P+ buffer (GE Healthcare). The surface was regenerated by three 60-s injections of 1 M NaCl. All data were analyzed with the Biacore T100 evaluation software version 2.0, with a 1:1 Langmuir binding model.

Crystallization and Structural Determination of KWAR23/SIRPα IgV Complex. KWAR23 Fab/SIRPα complexes were concentrated to 25 mg/mL in HBS. Crystals were obtained by addition of 0.1 μL of protein to an equal volume of 22% PEG3350, 150 mM ammonium sulfate, and 0.1 M Tris (pH 7.0), and were cryoprotected in mother liquor supplemented with 15% ethylene glycol. Diffraction studies were performed at beamline 12.2 at SLAC National Accelerator Laboratory. Diffraction data were processed with HKL-2000 (46). The KWAR23/SIRPα IgV complex was solved by molecular replacement with the individual model of the SIRPα IgV domain from the Protein Data Bank (accession code 2JJS) and the Fab from the Protein Data Bank. Refinement was carried out using PHENIX (47), and model adjustment was performed with Coot (48). Initial refinement used rigid body, coordinate, and real-space refinement, along with individual atomic displacement parameter refinement. Translation–Libration–Screw (TLS) refinement was added in later refinement iterations. Data collection and refinement statistics are given in Table S1.

Cell Isolation. Human peripheral blood samples were provided by the Stanford Blood Center. Human peripheral blood mononuclear cells were obtained by density gradient centrifugation using Ficoll-Paque (GE Healthcare Life Sciences), and human monocytes were isolated using human CD14 MicroBeads and LS columns (Miltenyi Biotec). Human neutrophils were isolated by density gradient centrifugation. Briefly, 25 mL of blood was mixed with 5 mL of acid-citrate-dextrose. Next, 15 mL of 6% dextran/sodium chloride solution was added, mixed, and left for 60 min at room temperature. The top layer containing leukocyte-rich plasma was aspirated and transferred to a new 50-mL conical tube. PBS was added up to 50 mL, and the cells were centrifuged at 200 × *g* for 12 min. Red blood cells were lysed by resuspending the cell pellet in 6 mL of ice-cold distilled water for 20 s. PBS was added, and the cells were centrifuged at 250 × *g* for 7 min. Mononuclear cells were removed by density gradient centrifugation (365 × *g* for 30 min) using Ficoll-Paque. Dead cells were excluded from the analysis by staining with DAPI (Sigma–Aldrich), and the purity was analyzed by an LSRFortessa flow cytometer (BD Biosciences).

Tumor Cells. Burkitt's lymphoma cells (Raji), breast cancer cells (SK-BR-3), colon adenocarcinoma cells (DLD-1, LS-174T, HT-29, and HCT-116), and renal carcinoma cells (Caki-1) were obtained from the American Type Culture Collection (ATCC). The renal carcinoma cell lines RCC4, RCC10, and TK10 were a gift from Amato J. Giaccia (Division of Radiation and Cancer Biology, Department of Radiation Oncology, Stanford University Medical Center, Stanford, CA) (49). Tumor cell lines were cultured in RPMI 1640 (Thermo Fisher Scientific), McCoy's 5A (modified) medium (Thermo Fisher Scientific), or complete DMEM (GE Healthcare Life Sciences), and supplemented with 10% FBS, 1% penicillin/streptomycin, and 4 mM L-alanyl-L-glutamine. Human macrophages and neutrophils were cultured in Iscove's Modified Dulbecco's Medium (IMDM) supplemented with 10% human serum (Thermo Fisher Scientific). All cell lines and assay cultures were maintained at 37 °C and 5% CO_2.

Cell Labeling. The fluorescent dye CFSE (Thermo Fisher Scientific) was used at a concentration of 1:5,000 to label tumor cells for the phagocytosis and cytotoxicity assays, as described previously (50).

Design of Bispecific Macrophage-Enhancing Antibodies. Gene block fragments of the V-regions of rituximab and vorsetuzumab, followed by those of KWAR23, in the dual variable domain-Ig format were ordered from IDT and cloned by Gibson assembly into pFUSE-Ig vectors from InVivoGen. The sequences used are described in Table S2.

Therapeutic Antibodies. The anti-human SIRPα antibody KWAR23 was used at a concentration of 10 μg/mL (in vitro) or 10 mg/kg (in vivo). Anti-CD20 antibodies (rituximab; Genentech and obinutuzumab; Roche), human anti-CD20 isotype collection (Invivogen), anti-EGFR antibodies (cetuximab; Bristoll-Myers Squibb and panitumumab; Amgen), anti-HER2 antibody (trastuzumab; Genentech), anti-CD70 antibody (vorsetuzumab; Seattle Genetics), and the bispecific anti-CD70/KWAR23 antibody were used at a concentration of 10 μg/mL (in vitro) or 10 mg/kg (in vivo) unless otherwise noted. The specificity of KWAR23 for human SIRPα was further tested by a competition assay to evaluate blockade of SIRPα on the surface of THP-1 cells. THP-1 cells were incubated with Alexa Fluor 647-conjugated human CD47 tetramers in the presence of varying concentrations of KWAR23.

Phagocytosis Assay. In vitro phagocytosis assays were performed by coculture of 5×10^4 human macrophages with 1×10^5 CFSE-labeled tumor cells for 2 h in serum-free IMDM. Phagocytosis was analyzed by an LSRFortessa flow cytometer. The percentage of $CFSE^+$ macrophages was calculated and normalized to the maximal response by each independent donor against each cell line using FlowJo software (TreeStar).

Cytotoxicity Assay. A total of 2.5×10^5 neutrophils were cocultured with 5×10^3 CFSE-labeled tumor cells for 4 h in RPMI 1640 supplemented with 10% human serum, 10 ng/mL granulocyte colony-stimulating factor (Peprotech), and 50 ng/mL recombinant human IFN-γ (Biolegend). The cells were analyzed by an LSRFortessa flow cytometer, and the percent relative cytotoxicity was determined using FlowJo software.

Mice. The generation of knockin mice encoding human *SIRPA* in a 129× BALB/c genetic background was performed in collaboration with Regeneron Pharmaceuticals using VelociGene technology (51). The mice were crossed to a *Rag2*$^{-/-}$ *Il2rg*$^{-/-}$ background (SRG mice) and were maintained under specific pathogen-free conditions. All animal studies were performed in compliance with Yale Institutional Animal Care and Use Committee protocols.

Tumor Inoculation and Antibody Therapy in SRG Mice. A total of 5×10^6 human Burkitt's lymphoma cells (Raji) were injected s.c. into SRG mice. Upon development of a visible tumor, ~14 d postinjection, mice received i.p. injections of PBS, anti-human CD20 antibody (rituximab; 10 mg/kg), anti-human SIRPα antibody (10 mg/kg), anti-human CD70 antibody (10 mg/kg), or bispecific anti-human CD70/KWAR23 (10 mg/kg) antibody every other day. Depletion of neutrophils by an anti-Ly6G antibody (0.2 mg per mouse) or phagocytic cells by clodronate (0.5 mg per mouse) was achieved by three injections before the start of the treatment with therapeutic antibodies (Fig. 5*A* and Fig. S3*A*). The depletion efficacy of target immune cells was determined by retroorbital blood collection and flow cytometric analysis before and at the end of treatment with therapeutic antibodies. The tumor volume was determined by caliper measurement and calculated using the following equation (52): Tumor Volume (mm^3) = 0.5 × (length × $width^2$). Tumor-infiltrating immune cells were isolated from the tumor xenograft using 10% FBS/RPMI 1640 supplemented with 1 mg/mL Collagenase D in a shaker for 45 min at 37 °C.

Flow Cytometry. The analysis of surface molecules was performed using monoclonal antibodies from Biolegend. The following anti-mouse antibodies were used: CD11b (clone: M1/70), CD11c (N418), CD45 (30-F11), CD172a (SIRPα; P84), F4/80 (BM8), Gr-1 (RB6-8C5), Ly6C (HK1.4), and Ly6G (1A8). The following anti-human antibodies were used: CD45 (HI30), CD172a (SIRPα; SE5A5), and CD206 (15-2). Data were acquired by LSRII or LSRFortessa flow cytometers and analyzed using FlowJo software.

Immunofluorescence Staining. Burkitt's lymphoma from SRG mice treated with rituximab and KWAR23 antibody were collected and fixed overnight in 4% paraformaldehyde, transferred to 30% sucrose the following day, embedded in O.C.T. compound (Tissue-Tek), snap-frozen, and stored at −80 °C. Sections of the tumors (8–10 μm) were cut on a CM1850 cryostat (Leica Biosystems) and transferred to glass slides (Fisher Scientific). The tissue sections were stained with the following primary antibodies: mouse anti-human CD45 (2D1; Biolegend), rat anti-mouse F4/80 FITC (BM8; Biolegend), and biotinylated recombinant human anti-mouse Ly6G (REA526; Miltenyi Biotec). Goat anti-rat AF488 (Molecular Probes), goat anti-mouse IgG AF594 (Molecular Probes), and streptavidin-AF647 (Life Technologies) were used

as secondary antibodies. Nuclei were stained with DAPI. The tumor sections were analyzed on a DMI6000 B epifluorescence microscope (Leica Biosystems).

Statistical Analysis. Statistical analysis was performed using Prism 7 software (GraphPad) and a two-tailed unpaired Student's *t* test.

ACKNOWLEDGMENTS. We thank Jon Alderman, Caroline Lieber, Theresa Storm, Linda Quinn, and Elizabeth Hughes-Picard for administrative assistance. N.G.R. and B.M.G. were supported by a Howard Hughes Medical Institute Medical Research Fellowship, D.H.-B. was supported by an Erwin Schrödinger Fellowship (Austrian Science Fund; Grant J3220-B19), K.W. was supported by the Stanford Medical Scientist Training Program Grant T32 GM07365, and L.S. was supported by a Mathilde Krim Fellowship (amfAR, The Foundation for AIDS Research) and by NIH Grants 1K99AI125065-01 and T32 AI07019. This work was supported, in part, by the Bill and Melinda Gates Foundation and the Howard Hughes Medical Institute (R.A.F.).

1. Blattman JN, Greenberg PD (2004) Cancer immunotherapy: A treatment for the masses. *Science* 305:200–205.
2. Mellman I, Coukos G, Dranoff G (2011) Cancer immunotherapy comes of age. *Nature* 480:480–489.
3. Larkin J, et al. (2015) Combined nivolumab and ipilimumab or monotherapy in untreated melanoma. *N Engl J Med* 373:23–34.
4. Reck M, et al.; KEYNOTE-024 Investigators (2016) Pembrolizumab versus chemotherapy for PD-L1-positive non-small-cell lung cancer. *N Engl J Med* 375:1823–1833.
5. Obenauf AC, et al. (2015) Therapy-induced tumour secretomes promote resistance and tumour progression. *Nature* 520:368–372.
6. Pitt JM, et al. (2016) Resistance mechanisms to immune-checkpoint blockade in cancer: Tumor-intrinsic and -extrinsic factors. *Immunity* 44:1255–1269.
7. Perdiguero EG, Geissmann F (2016) The development and maintenance of resident macrophages. *Nat Immunol* 17:2–8.
8. Ugel S, De Sanctis F, Mandruzzato S, Bronte V (2015) Tumor-induced myeloid deviation: When myeloid-derived suppressor cells meet tumor-associated macrophages. *J Clin Invest* 125:3365–3376.
9. Elinav E, et al. (2013) Inflammation-induced cancer: Crosstalk between tumours, immune cells and microorganisms. *Nat Rev Cancer* 13:759–771.
10. Condamine T, Ramachandran I, Youn JI, Gabrilovich DI (2015) Regulation of tumor metastasis by myeloid-derived suppressor cells. *Annu Rev Med* 66:97–110.
11. Gebhardt C, et al. (2015) Myeloid cells and related chronic inflammatory factors as novel predictive markers in melanoma treatment with ipilimumab. *Clin Cancer Res* 21: 5453–5459.
12. Wculek SK, Malanchi I (2015) Neutrophils support lung colonization of metastasis-initiating breast cancer cells. *Nature* 528:413–417.
13. Coffelt SB, et al. (2015) IL-17-producing γδ T cells and neutrophils conspire to promote breast cancer metastasis. *Nature* 522:345–348.
14. Jaiswal S, et al. (2009) CD47 is upregulated on circulating hematopoietic stem cells and leukemia cells to avoid phagocytosis. *Cell* 138:271–285.
15. Brown EJ, Frazier WA (2001) Integrin-associated protein (CD47) and its ligands. *Trends Cell Biol* 11:130–135.
16. Adams S, et al. (1998) Signal-regulatory protein is selectively expressed by myeloid and neuronal cells. *J Immunol* 161:1853–1859.
17. Barclay AN, Van den Berg TK (2014) The interaction between signal regulatory protein alpha (SIRPα) and CD47: Structure, function, and therapeutic target. *Annu Rev Immunol* 32:25–50.
18. Herndler-Brandstetter D, et al. (October 25, 2017) Humanized mouse model supports development, function and tissue residency of natural killer cells. *Proc Natl Acad Sci USA* 114(45):E9626–E9634.
19. Darcy PK, Neeson P, Yong CS, Kershaw MH (2014) Manipulating immune cells for adoptive immunotherapy of cancer. *Curr Opin Immunol* 27:46–52.
20. Goodwin RG, et al. (1993) Molecular and biological characterization of a ligand for CD27 defines a new family of cytokines with homology to tumor necrosis factor. *Cell* 73:447–456.
21. Croft M (2009) The role of TNF superfamily members in T-cell function and diseases. *Nat Rev Immunol* 9:271–285.
22. Law CL, et al. (2006) Lymphocyte activation antigen CD70 expressed by renal cell carcinoma is a potential therapeutic target for anti-CD70 antibody-drug conjugates. *Cancer Res* 66:2328–2337.
23. McEarchern JA, et al. (2007) Engineered anti-CD70 antibody with multiple effector functions exhibits in vitro and in vivo antitumor activities. *Blood* 109:1185–1192.
24. Batlevi CL, Matsuki E, Brentjens RJ, Younes A (2016) Novel immunotherapies in lymphoid malignancies. *Nat Rev Clin Oncol* 13:25–40.
25. Scott AM, Wolchok JD, Old LJ (2012) Antibody therapy of cancer. *Nat Rev Cancer* 12: 278–287.
26. Khalil DN, Smith EL, Brentjens RJ, Wolchok JD (2016) The future of cancer treatment: Immunomodulation, CARs and combination immunotherapy. *Nat Rev Clin Oncol* 13: 273–290.
27. Weiskopf K (2017) Cancer immunotherapy targeting the CD47/SIRPα axis. *Eur J Cancer* 76:100–109.
28. Inagaki K, et al. (2000) SHPS-1 regulates integrin-mediated cytoskeletal reorganization and cell motility. *EMBO J* 19:6721–6731.
29. Zhao XW, et al. (2011) CD47-signal regulatory protein-α (SIRPα) interactions form a barrier for antibody-mediated tumor cell destruction. *Proc Natl Acad Sci USA* 108: 18342–18347.
30. Yanagita T, et al. (2017) Anti-SIRPα antibodies as a potential new tool for cancer immunotherapy. *JCI Insight* 2:e89140.
31. Maloney DG, et al. (1997) IDEC-C2B8 (Rituximab) anti-CD20 monoclonal antibody therapy in patients with relapsed low-grade non-Hodgkin's lymphoma. *Blood* 90: 2188–2195.
32. Liu X, et al. (2015) CD47 blockade triggers T cell-mediated destruction of immunogenic tumors. *Nat Med* 21:1209–1215.
33. Tseng D, et al. (2013) Anti-CD47 antibody-mediated phagocytosis of cancer by macrophages primes an effective antitumor T-cell response. *Proc Natl Acad Sci USA* 110: 11103–11108.
34. Chen J, et al. (2017) SLAMF7 is critical for phagocytosis of haematopoietic tumour cells via Mac-1 integrin. *Nature* 544:493–497.
35. Nicolás-Ávila JA, Adrover JM, Hidalgo A (2017) Neutrophils in homeostasis, immunity, and cancer. *Immunity* 46:15–28.
36. Qian BZ, Pollard JW (2010) Macrophage diversity enhances tumor progression and metastasis. *Cell* 141:39–51.
37. Highfill SL, et al. (2014) Disruption of CXCR2-mediated MDSC tumor trafficking enhances anti-PD1 efficacy. *Sci Transl Med* 6:237ra67.
38. Franklin RA, et al. (2014) The cellular and molecular origin of tumor-associated macrophages. *Science* 344:921–925.
39. Gajewski TF, Schreiber H, Fu YX (2013) Innate and adaptive immune cells in the tumor microenvironment. *Nat Immunol* 14:1014–1022.
40. Schumacher TN, Schreiber RD (2015) Neoantigens in cancer immunotherapy. *Science* 348:69–74.
41. Salmon H, et al. (2016) Expansion and activation of CD103(+) dendritic cell progenitors at the tumor site enhances tumor responses to therapeutic PD-L1 and BRAF inhibition. *Immunity* 44:924–938.
42. Schmid MC, Varner JA (2010) Myeloid cells in the tumor microenvironment: Modulation of tumor angiogenesis and tumor inflammation. *J Oncol* 2010:201026.
43. De Henau O, et al. (2016) Overcoming resistance to checkpoint blockade therapy by targeting PI3Kγ in myeloid cells. *Nature* 539:443–447.
44. Massagué J, Obenauf AC (2016) Metastatic colonization by circulating tumour cells. *Nature* 529:298–306.
45. Weiskopf K, et al. (2013) Engineered SIRPα variants as immunotherapeutic adjuvants to anticancer antibodies. *Science* 341:88–91.
46. Minor W, Cymborowski M, Otwinowski Z, Chruszcz M (2006) HKL-3000: The integration of data reduction and structure solution–From diffraction images to an initial model in minutes. *Acta Crystallogr D Biol Crystallogr* 62:859–866.
47. Terwilliger TC, et al. (2008) Iterative model building, structure refinement and density modification with the PHENIX AutoBuild wizard. *Acta Crystallogr D Biol Crystallogr* 64:61–69.
48. Emsley P, Cowtan K (2004) Coot: Model-building tools for molecular graphics. *Acta Crystallogr D Biol Crystallogr* 60:2126–2132.
49. Razorenova OV, et al. (2011) VHL loss in renal cell carcinoma leads to up-regulation of CUB domain-containing protein 1 to stimulate PKC{delta}-driven migration. *Proc Natl Acad Sci USA* 108:1931–1936.
50. Jedema I, van der Werff NM, Barge RM, Willemze R, Falkenburg JH (2004) New CFSE-based assay to determine susceptibility to lysis by cytotoxic T cells of leukemic precursor cells within a heterogeneous target cell population. *Blood* 103:2677–2682.
51. Valenzuela DM, et al. (2003) High-throughput engineering of the mouse genome coupled with high-resolution expression analysis. *Nat Biotechnol* 21:652–659.
52. Bullard DE, Schold SC, Jr, Bigner SH, Bigner DD (1981) Growth and chemotherapeutic response in athymic mice of tumors arising from human glioma-derived cell lines. *J Neuropathol Exp Neurol* 40:410–427.